Atmospheric Boundary Layer Characterization Using Multiyear Ground-Based Microwave Radiometric Observations Over a Tropical Coastal Station

R. Renju, C. Suresh Raju, M. K. Mishra, N. Mathew, K. Rajeev, and K. Krishna Moorthy

***Abstract*— The continuous ground-based microwave radiometer profiler (MRP) observations of lower atmospheric temperature and humidity profiles are used to investigate the diurnal evolution of atmospheric boundary layer height (BLH) over a tropical coastal station. The BLH estimated from the MRP observations is compared with concurrent and collocated measurements of mixing layer height using a Micropulse Lidar and the BLH derived from radiosonde ascends. The monthly mean diurnal variation of the BLH derived from the multiyear (2010–2013) MRP observations exhibits strong diurnal variation with the highest around the local afternoon (∼12:00–15:00 IST) and the lowest during the nighttime (∼100–200 m). The daytime convective BLH is maximum during the premonsoon season (March–May) with the peak value (∼1300 m) occurring in April and minimum in the month of July (∼600 m). This paper presents the potential of MRP observations to investigate the continuous diurnal evolution of the BLH over a tropical coastal region manifested by a thermal internal boundary layer (TIBL) at much better time resolution, which is essential for understanding the rapid growth of the boundary layer and the TIBL during the forenoon period.**

***Index Terms*— Microwave radiometry, terrestrial atmosphere.**

I. Introduction

THE atmospheric boundary layer (ABL) is the lowest part of the atmosphere that acts as a conduit for the transfer of constituents (including water vapor and pollutants), energy (sensible and latent heat), and momentum between the surface and the free-troposphere, and it has immense significance in atmospheric science and air pollution studies [1]. The boundary layer height (BLH) is one of the crucial parameters of the ABL, primarily determines the volume of air mass available for pollutant dispersal and their exchange with the free troposphere, and is an important parameter in numerical weather prediction models [1]. The ABL height over land undergoes considerable diurnal evolution, which depends on the prevailing meteorological and geographical conditions. Soon after the sunrise, rapid heating of land results in a thermal gradient between land and ocean in the coastal regions, leading to the onset of the mesoscale sea breeze (SB) circulation besides an increase in the vertical extent of convection, during which the convective eddies constantly stir the atmosphere [2]. With the onset of the SB, cool air from the oceanic environment advects over the land and modifies the prevailing vertical temperature structure over the coast, leading to the formation of thermally modified internal boundary layer. The reverse process occurs after the sunset, leading to the onset of land breeze (LB) during the night and early morning period. These processes further modulate the development of daytime convective boundary layer (CBL) and the nighttime stable boundary layer (SBL) over coastal regions [1].

The BLH cannot be directly measured, but can be estimated from the altitude profiles of parameters, such as mechanical turbulence, temperature, humidity, aerosol concentration, or atmospheric refractive index. Using radiosonde observations, the BLH is determined by the temperature inversion and associated sharp negative gradient in humidity and can also be derived using the parcel method as the altitude up to which the surface air at a given temperature can rise adiabatically through convection [3]. Using the vertical gradient of virtual potential temperature (θ_v) and the bulk Richardson number [4], top of the CBL can also be identified. Since radiosonde ascents are limited to specific times of a day, they are not adequate for studying the continuous diurnal evolution of the BLH. The remote sounding systems, such as lidar, sodar, radio acoustic sounding system, and wind profiling radars, provide continuous measurements of the atmospheric parameters, but the demarcation of the BLH may not be clear every time in the wind profile. In the case of sodar [5], the maximum detectable height is mostly limited to below 1 km and is also sensitive to environmental noise. Lidar backscatter profiles can be used to derive the vertical distribution of the aerosols (in terms of aerosol backscattering coefficient) in the atmosphere. Using the aerosols as tracers, the mixing height can be determined as the region above which aerosol concentration shows a sharp gradient [6]. However, limitations in this method arise because of the occurrence of fair weather clouds and the advection of aerosols. The refractivity profiles observed using GPS radio occultation technique also

Manuscript received November 25, 2016; revised March 28, 2017 and June 13, 2017; accepted July 31, 2017. Date of publication September 4, 2017; date of current version November 22, 2017. *(Corresponding author: C. Suresh Raju.)*

R. Renju, C. Suresh Raju, M. K. Mishra, N. Mathew, and K. Rajeev are with the Space Physics Laboratory, Thiruvananthapuram 695022, India (e-mail: c_sureshraju@vssc.gov.in).

K. Krishna Moorthy is with the Indian Institute of Science, Bengaluru 560012, India.

Color versions of one or more of the figures in this paper are available online at http://ieeexplore.ieee.org.

Digital Object Identifier 10.1109/TGRS.2017.2735626

provide reliable information on the BLH [7]. However, these measurements are highly limited in space and time.

Microwave radiometric observations offer continuous profiling of atmospheric temperature and humidity in lower atmosphere and are used for investigating the diurnal evolution of the ABL and their intercomparison with other techniques at various locations. Diurnal variability of the thermodynamic state of the ABL during cold front passage had been carried out using radiometric observations over Lindenberg [8]. As a part of African Monsoon Multidisciplinary Analysis Project, the inland boundary layer features and their variabilities were studied [9]. The determination of the mixing layer height (MLH) in a semiurban environment from the ground-based microwave brightness temperature was reported [10]. Most of these studies using microwave radiometer profiler (MRP) were carried out in high and midlatitude regions. The MRP observations are extensively being used over the Indian region for convective and water vapor studies [11]. But the potential of MRP for the investigation of the coastal boundary layer over the tropical region has not been explored so far. Thus, the main objective of this paper is to explore the potential of MRP data to characterize the seasonal mean diurnal variation of the ABL over a coastal station.

II. Experimental Location, Data, and Methodology

A. Experimental Location

The experiment site is at Thumba, Thiruvananthapuram (TVM: 8.5°N, 76.9°E, 6 m amsl), a coastal station (∼500 m from the Arabian Sea coast) located at the southwestern coast of the Indian peninsula. Based on the prevailing synoptic meteorological conditions, the station experiences four seasons: winter (December–February), premonsoon (March–May), summer monsoon (June–September), and postmonsoon (October–November). Dry weather prevails during winter, while convective conditions with isolated precipitation occur during pre- and postmonsoon seasons. The station is located in the gateway region of the southwest summer monsoon to the Indian subcontinent and experiences widespread clouds and rain during June–September. SB/LB circulations prevail during most part of the year except during the summer monsoon season, which is manifested by strong south westerly winds.

B. Microwave Radiometer Profiler

The MRP (model of MP: 3000A) has been in regular operation at the station since April 2010. Details of the study region, MRP system characteristics, and the method of data analysis are detailed by Raju *et al.* [12]. The MRP measures brightness temperatures through a sequential scan of eight frequencies in the K-band (22.23–30.0 GHz) and 14 frequencies in the V-band (51.2–58.8 GHz) with a bandwidth of 300 MHz for each channel. The resonant channels have maximum contribution from the lower altitudes and hence can provide humidity and temperature profiles with high resolution at lower altitudes, which makes it suitable for boundary layer studies. Apart from microwave sensors, the MRP also includes meteorological sensors for the measurement of ambient pressure, temperature, and humidity and an IR radiometer to measure cloud base temperature. The K-band channels are calibrated to 0.3 K rms by automated tipping procedures [13] and V-band channels are calibrated to 1.5 K rms with liquid nitrogen target [14]. The all-weather capability of MRP facilitates [15] continuous measurements of temperature and humidity profiles with a temporal resolution of ∼3 min under multiangle elevation scan mode. The retrieval of atmospheric parameters is made in the vertical grid spacing of ∼50, 100, and 250 m at <500 m, 500–2000 m, and >2000 m, respectively. The neural network technique has been used to retrieve the atmsopheric profiles, which has been trained with data set of radiosonde profiles covering ten years of climatology over the TVM region.

In this paper, the MRP data are used to determine the BLH using the parcel method, where the height of intersection of the actual virtual potential temperature (θ_v) profile with the dry-adiabatic ascent starting at near-surface θ_v is determined as the BLH [16]. It is found that this method is in agreement with the θ_v gradient method, where the MLH is defined at an altitude where the vertical gradient in θ_v exceeds 3 K/km. A strict quality control was adopted to select the clear sky (cloud free) condition profiles by applying an IR temperature threshold, <270 K (IR radiometer attached to the MRP). In this process, 504 days (out of 708 nonrainy days) were identified as clear sky days with maximum number of days in the winter (166) and minimum in the monsoon period (112).

C. Lidar Data and Method of Analysis

A collocated Micropulse Lidar (MPL) has been in operation during the MRP measurements. The system details, the method of data processing, inversion of the data to retrieve aerosol backscatter coefficient, and linear depolarization ratio (LDR) are described by other authors [17]. The MPL consists of a diode-pumped Nd: YAG laser as transmitter emits pulses of 7 ns width at 532-nm wavelength at a rate of 2500 Hz. The system has a range resolution of 30 m and time integration of 60 s. The aerosol concentration decreases significantly with altitude above the boundary layer, resulting in a strong altitude gradient of aerosol concentration across the top of the mixed layer. Hence, the mixed layer can be determined from lidar measurements as the height at which sudden decrease in lidar signal strength with altitude occurs. A quantitative analysis of MLH is carried out using the vertical gradient and temporal variations of the normalized attenuated backscattered signal (NABS) and LDR derived from the lidar data. The altitude at which the filtered first-order derivative of NABS with respect to altitude [d(NABS)/dz] turns negative is considered as MLH [18]. The vertical gradient of LDR [d(LDR)/dz] and its time evolution has also been taken for deriving MLH.

D. Radiosonde Observations

The *i-met* balloon-borne radiosondes were launched on a few days from Thumba to derive the altitude profiles of temperature (±0.5 °C accuracy), relative humidity (5% accuracy),

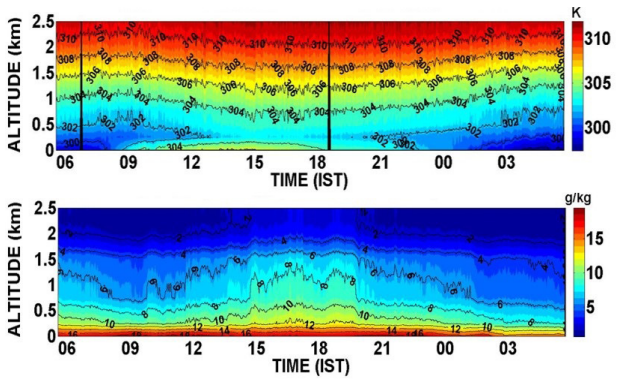

Fig. 1. Time–height variation of (Top) virtual potential temperature and (Bottom) water vapor mixing ratio during January 19 and 20, 2011 derived from MRP observations. Black lines indicate time of sunrise and sunset.

and zonal *(u)* and meridional *(v)* wind components (accuracy of 1 m/s). These data are used for determining the BLH over the site using the vertical gradient of θ_v and water vapor mixing ratio *(r)*. The local coastline is roughly aligned along 145°–325°; the winds blowing between 145° and 325° constitute the SB, while the seaward winds blowing between 325° and 145° constitute the LB over the study region. Wind components perpendicular to the coastline are resolved to enable the measurement of SB strength. Positive (negative) values of SB component (SBC) indicate the SB (LB).

III. Results

A. Boundary Layer Structure Evolution

The time–height cross sections of θ_v and r between the surface and 2.5 km derived from MRP data on January 19 and 20, 2011 (Fig. 1) show that θ_v continuously increases with altitude during the night and morning hours (∼23–08 IST), which characterizes the SBL conditions. Stability is strongest during the early morning period when the surface temperature attains its minimum. The CBL develops after 08–09 IST, where θ_v decreases with an increase in altitude between the surface and ∼300 m above which neutral conditions prevail. Strength (upper altitude limit and temperature) of this CBL increases between ∼09 and ∼15 IST. Values of θ_v near the surface are comparable to those at ∼950 m during 12–16 IST, indicating that the air parcel at the surface can get well-mixed up to ∼1-km altitude, which represents the BLH during the daytime conditions. A strong capping inversion layer with virtual potential temperature lapse rate of >3 K/km prevails above the CBL. The response of the atmospheric mixing processes to the altitude variation of θ_v is well manifested in the diurnal evolution of water vapor mixing ratio [Fig. 1 (top)], which shows a rapid decrease with altitude right from the surface during late night and early morning period. Associated with the development of the daytime CBL, water vapor gets well mixed to the upper layers up to ∼700 m to >1 km during 12–18 IST. Here, the tracer is the water vapor whose vertical gradient shows higher BLH values compared with those inferred from θ_v as the water vapor gets convectively mixed up to slightly above the thermal inversion. Water vapor transported to the upper part of the CBL prevails there even after the cessation of the thermals and the setting up of surface stable layer after the sunset. This is because water vapor in the daytime convective layer resides in the residual layer (remnants of the daytime CBL) during the late evening, which prevails above the SBL. After the midnight, the water vapor get trapped mostly below ∼200 m till the early morning period.

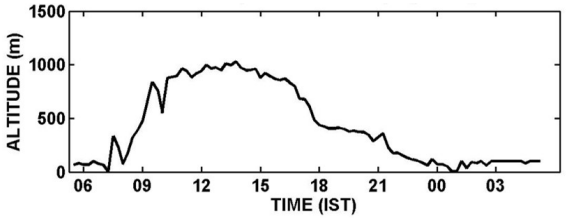

Fig. 2. Diurnal variation of BLH derived from MRP observations of virtual potential temperature during January 19 and 20, 2011.

Fig. 2 shows the BLH computed during January 19 and 20, 2011 from MRP data using a parcel method. The CBL rapidly develops after ∼09 IST when the BLH increases from <200 m during the postmidnight and morning period to attain the maximum value of ∼1000 m at 13–14 IST. Associated with the decrease in thermals, the convective BLH systematically decreases after ∼15 IST to ∼500 m during 18–21 IST and to <200 m during the postmidnight period.

B. Intercomparison of BLH Derived From MRP, MPL, and Radiosonde

Intercomparison of the BLH derived from MRP observations during January 19 and 20, 2011 with those estimated from the concurrent and colocated MPL and radiosonde observations has been carried out. The time–height cross sections of the ABS and LDR derived from MPL observations during January 19–21, 2011 are shown in Fig. 3. The altitude gradient of the ABS shows that most of the aerosols are concentrated in the lower altitude levels below ∼500 m during the postmidnight and morning period when the SBL prevails. As the CBL builds up during the daytime, the aerosols are dispersed progressively deeper into layers resulting in increased ABS (and aerosol concentration) at higher altitudes up to ∼1500 m, which indicate the height of the mixed layer. Relatively nonspherical aerosols prevailing near the surface are dispersed to higher altitudes during the development of the CBL. This is clearly seen from the time–height cross section of LDR, which shows larger values of LDR (>0.04) after ∼09 IST at higher altitudes, especially up to ∼1500 m. The MLH derived from the ABS matches well with that inferred from the time–height variation of LDR.

Note that MRP and MPL use distinctly different parameters as tracers for estimating the BLH. The MLH derived from MPL data shows a maximum MLH extending to ∼1500 m, which is higher than the BLH derived from the MRP observations (∼1000 m). This difference arises mainly due to the different physical processes governing the two tracers. During the clear sky days with intense solar heating, the turbulent eddies

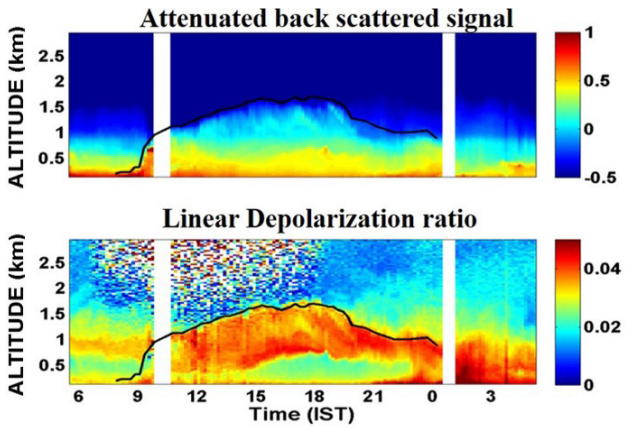

Fig. 3. Time–height cross section of (Top) attenuated lidar backscattered signal and (Bottom) LDR observed using Micropulse lidar during January 19 and 20, 2011. The black line shows the MLH estimated from lidar backscattered signal.

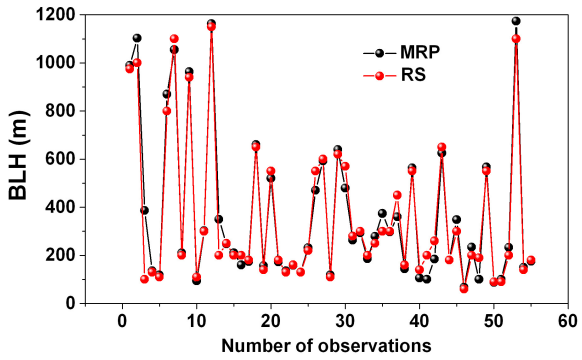

Fig. 4. BLH computed from MRP (black circles) and collocated radiosonde (red circles) is compared for 55 ascends in 2011.

slightly overshoot the inversion layer at the ABL top resulting in deeper mixing of aerosols (Fig. 3). This is also evident in the deeper mixing observed in water vapor [Fig. 1 (bottom)]. While the BLH derived from MRP indicates the ABL top from the thermal inversion using parcel method that estimated from the MPL shows the aerosol mixing height. Furthermore, the aerosols and water vapor transported to the upper layer of the daytime CBL reside there (residual layer) even after the cessation of thermals. The decrease in aerosol and water vapor concentration in the residual layer and their confinement to <500 m occurs only during the postmidnight period. Similarly, the response of water vapor and aerosol distribution to thermal eddies result in the differences observed in the times at which the respective layer heights peak: the MLH derived from MPL observations peaks at ∼15–18 IST, whereas the BLH derived from parcel method peaks at ∼13–15 IST.

In the backdrop of the above, the MRP derived BLH is compared with that derived from the concurrent radiosonde measurements of temperature and humidity. Fig. 4 shows the comparison between the BLH estimated from radiosonde observations, which are computed following the θ_v gradient method for 55 collocated radiosonde ascents obtained for different times from 02:30 LT to 23:30 LT, and that from MRP. The linear regression between the two measurements yields correlation coefficient ∼0.95 (slope:∼0.9; intercept:∼10 m) and standard deviation ∼50 m. The uncertainity can be attributed to the limited vertical resolution, errors in retrieval of MRP observations, and uncertainity in the radiosonde measurements.

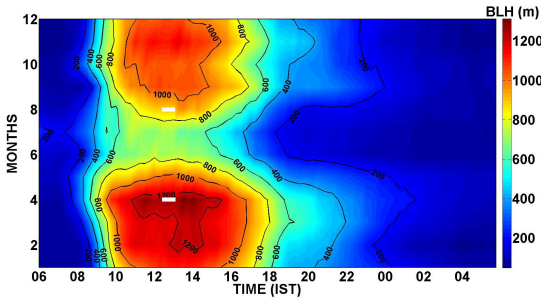

Fig. 5. Annual cycle of the monthly mean diurnal variation of BLH derived from multiyear (2010–2013) MRP observations.

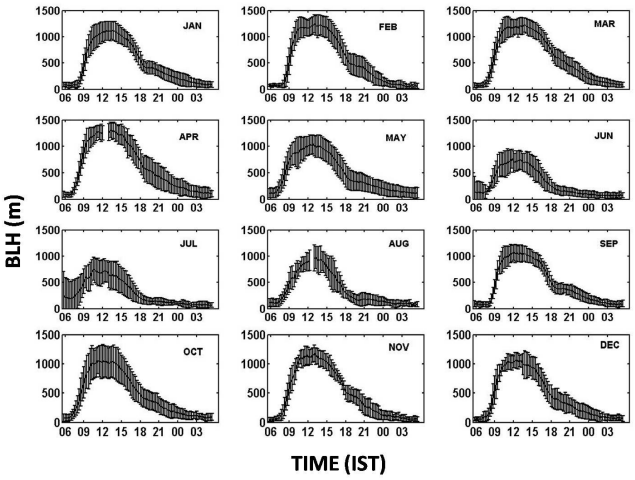

Fig. 6. Monthly mean diurnal variations of BLH and their corresponding standard deviations (vertical lines) derived from MRP data (2010–2013).

C. Diurnal Evolution of ABL at the Coastal Site

Being controlled strongly by the thermals (which depend directly on the solar insolation) and the LB/SB circulation, the diurnal evolution of the ABL at this coastal location is expected to exhibit characteristic signatures in the variations of atmospheric thermodynamic parameters. Diurnal variations of the BLH on monthly mean basis are estimated from MRP daily data during 2010–2013, by averaging the BLH values using an equivalent-day analysis and are shown as contour in Fig. 5. The corresponding monthly mean diurnal variations of the BLH with their standard deviations are depicted in Fig. 6.

In general, the diurnal evolution of the BLH during all the months is characterized by a shallow (<200 m) ABL during the postmidnight and early morning and a rapid growth of the CBL after 09 IST reaching the peak value before noon, which prevails until ∼15 IST. The BLH gradually decreases from the afternoon peak value after ∼15 IST. Subsequently the ABL gradually collapses into the nocturnal stable layer, which is quite shallow (< 200 m). On average, the development of the CBL is more rapid (∼30–450 m/h) during 08–11 IST compared with its decay (150–300 m/h) during ∼15–18 IST.

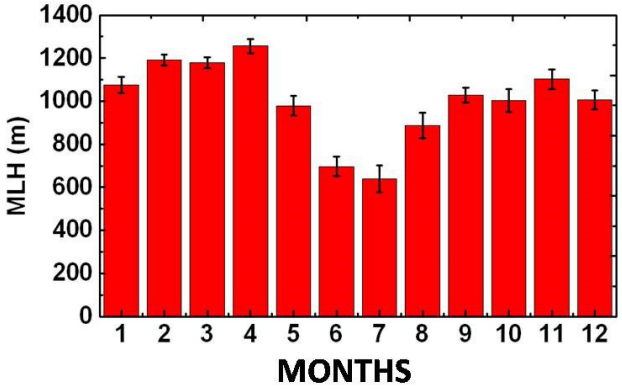

Fig. 7. Multiyear (2010–2013) monthly mean variation of daytime BLH peak value during January–December with standard deviation (vertical lines).

Further lowering of the BLH after the sunset is slower than that during the afternoon. Around the noon, the vertical motion of thermals attains maxima and the ABL depth remains somewhat similar (∼700–1200 m) during most of the afternoon period (12–15 IST). The maximum value of the BLH occurs in the month of April (∼1300 m). During the summer monsoon period, the development of the CBL is weaker with daytime peak BLH in the range of 600–800 m. It is smaller during June andJuly when the region has maximum cloudiness. The depth of nocturnal boundary layer varies in the range of 100–200 m during all months. The diurnal maximum of the BLH is attained around local noon and maintained for about 3–4 h. This is the time when maximum mixing of atmospheric constituents due to convective processes occurs. Average values of this the daytime peak BLH along with their standard deviations are shown in Fig. 7. The monthly mean values of the peak daytime BLH show systematic annual variability with values increasing from December (∼1000 m) to April (∼1300 m), followed by a decrease till July (∼600 m). These values show an increase from July till November.

D. Seasonal Mean Diurnal Variation of TIBL

Over the coastal region, the diurnal development of boundary layer is affected by the mesoscale circulation systems like LB/SB and the associated formation of TIBL which resides within the ABL [19]. When the air flows from a cooler surface to a warmer surface, a convective TIBL forms and it deepens as the turbulence increases. On the other hand, a stable TIBL forms when air flows from warmer to cooler surface. The formation of TIBL is evident from the diurnal variability of θ_v as shown in Fig. 1 (top). The formation of stable and unstable atmospheric layers are discernible in the gradient of θ_v, which indicate that at ∼09 IST the stable condition get transformed to unstable one and after ∼21 IST the reverse condition occurred.

The LBs/SBs play a major role in the temporal variation of the TIBL within the ABL. The diurnal variation of the SBC near the surface (1.6 m above ground level) during January 19, 2011 [Fig. 8 (top)] indicates that the SB onset occurs at ∼09 IST, while the LB sets in by ∼21 IST. The vertical gradient in θ_v shows that the formation of the TIBL is initiated with the onset of SB and more stable nocturnal boundary layer gets formed at ∼21 IST with the onset

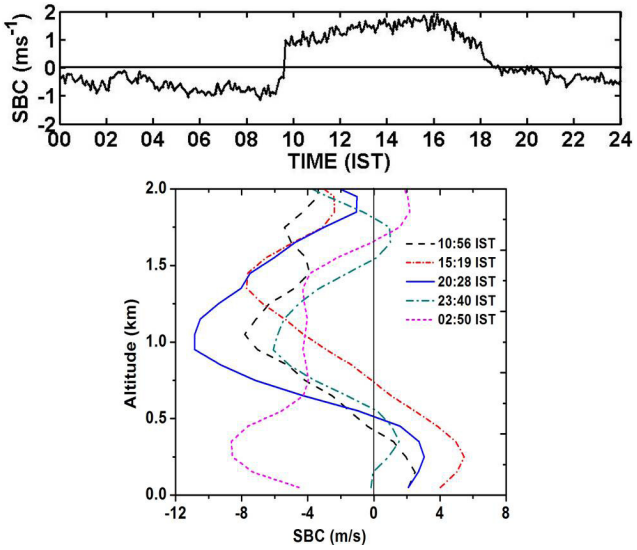

Fig. 8. (Top) Diurnal variation of SBC near surface on January 19, 2011 with positive values indicating SB and negative indicating LB. (Bottom) Altitude variation of SBC for five different times on January 19, 2011 observed using radiosonde.

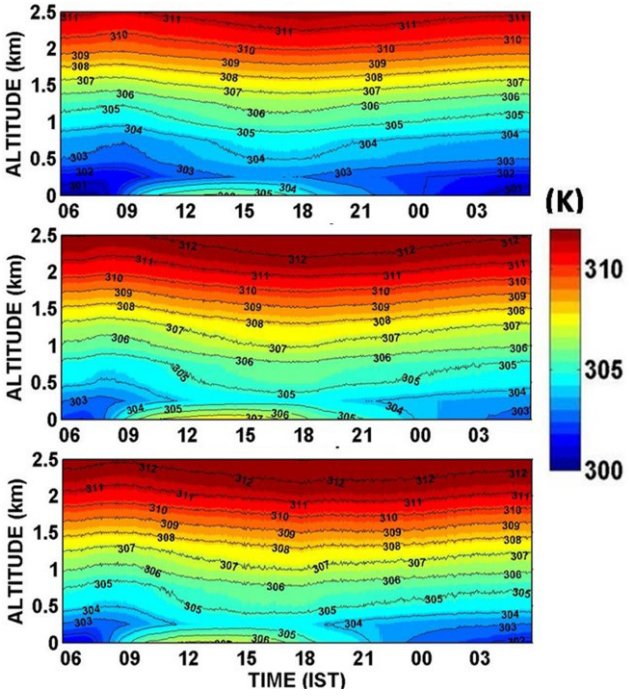

Fig. 9. Seasonal mean diurnal variability of virtual potential temperature is shown for (Top) winter (DJF), (Middle) premonsoon (MAM), and (Bottom) postmonsoon (ON) periods.

of LB. The vertical profiles of the SBC at five different times (obtained from radiosonde profiles) [Fig. 8 (bottom)] also indicate that the SBC is positive at 11, 15, and 20 IST and the altitude at which wind reversal takes place also increases with time from ∼400 m at ∼11 IST to ∼800 m at ∼15 IST, indicating formation and deepening of the convective TIBL. On the other hand, the LB regime dominates after ∼00 IST, which is manifested by the occurrence of an SBL observed using MRP. The altitude region of the SBC and its time variation seen in the radiosonde profiles of January 19, 2011

are in agreement with the altitude at which θ_v observed using MRP indicating a distinct increase during this day.

The multiyear observations during 2010–2013 have been utilized to understand the seasonal variability in the diurnal evolution of the TIBL over this region. Fig. 9 shows an equivalent day analysis of the time–height variation of θ_v over the study region, obtained by combining all the profiles obtained at the same local time (at 5-min bin) during all clear sky days during the respective seasons. The summer monsoon season is not included due to the prevailing synoptic scale sea-wind, which masks the TIBL or even inhibiting its formation. The winter period over the location is characterized with the TIBL formation by 09–10 IST and its depth varies from ∼200 m to ∼600 m during the course of the day. This unstable TIBL lasts for ∼9–10 h and diminishes by ∼21 IST [Fig. 9 (top)]. The existence of the TIBL is shorter during winter period compared with the pre- and postmonsoon seasons. During the premonsoon period, due to longer days and high surface temperature, the formation of unstable layer is prolonged and the TIBL persists for longer period ∼12–13 h [Fig. 9 (middle)]. During the postmonsoon period [Fig. 9 (bottom)], the TIBL formation is present for the duration of ∼12 h.

IV. Conclusion

The diurnal evolution of the coastal atmospheric BLH has been investigated using multiyear observations of high temporal resolution temperature and humidity profiles derived from MRP at a tropical coastal station, TVM located at the southwest peninsular India. The BLH deduced from MRP observations is compared with the BLH derived from radiosonde profiles showing good agreement, while MLHs derived from MPL are about 200–300 m higher than that of the BLH derived from the MRP observed temperature profiles. This is also confirmed by the vertical extent of mixing inferred from the water vapor mixing ratio profiles observed using MRP, which is in better agreement with the corresponding values of the MLH of aerosols observed using lidar. The seasonal mean diurnal variation of the BLH shows a systematic increase during 09–13 IST and a reduction after ∼15 IST. This variation is observed in all seasons. The peak value of the BLH is ∼1300 m during premonsoon, ∼1100 m during postmonsoon, and ∼900 m during winter season. The nocturnal BLH is 100–200 m during all seasons. The MRP observations also brought out the prominent signature of the TIBL caused by the SB circulation with the typical TIBL height (peak at ∼13–15 IST) of ∼500–600 m. This paper illustrates the potential of microwave remote sensing in determining the fine-scale variation of lower troposphere characteristics and continuous time evolution of the ABL height over tropical coastal region (manifested by internal boundary layer) at much better time resolution.

References

[1] R. B. Stull, Ed., *An Introduction to Boundary Layer Meteorology*. Dordrecht, The Netherlands: Kluwer, 1988.

[2] C. H. B. Priestley, *Turbulent Transfer in the Lower Atmosphere*. Chicago, IL, USA: Univ. Chicago Press, 1959.

[3] C. G. Holzworth, "Estimates of mean maximum mixing depths in the contiguous United States," *Monthly Weather Rev. Geophys.*, vol. 92, pp. 235–242, May 1964.

[4] A. Jeričević and B. Grisogono, "The critical bulk Richardson number in urban areas: Verification and application in a numerical weather prediction model," *Tellus A*, vol. 58, no. 1, pp. 19–27, 2006.

[5] F. Beyrich, "Mixing-height estimation in the convective boundary layer using sodar data," *Bound.-Layer Meteorol.*, vol. 74, nos. 1–2, pp. 1–18, 1995.

[6] K. Parameswaran, G. Vijayakumar, and B. V. K. Murthy, "Lidar observations on aerosol mixing height in a tropical coastal environment," *Indian J. Radio Space Phys.*, vol. 26, no. 1, pp. 15–21, 1997.

[7] A. von Engeln, J. Teixeira, J. Wickert, and S. A. Buehler, "Using CHAMP radio occultation data to determine the top altitude of the Planetary Boundary Layer," *Geophys. Res. Lett.*, vol. 32, no. 6, pp. L06815-1–L06815-4, 2005.

[8] J. Güldner and D. Spänkuch, "Remote sensing of the thermodynamic state of the atmospheric boundary layer by ground-based microwave radiometry," *J. Atmos. Ocean. Technol.*, vol. 18, pp. 925–933, Jun. 2001.

[9] B. Pospichal and S. Crewell, "Boundary layer observations in West Africa using a novel microwave radiometer," *Meteorologische Zeitschrift*, vol. 16, no. 5, pp. 513–523, 2007.

[10] D. Cimini, F. De Angelis, J.-C. Dupont, S. Pal, and M. Haeffelin, "Mixing layer height retrievals by multichannel microwave radiometer observations," *Atmos. Meas. Techn. Discuss.*, vol. 6, no. 3, pp. 4971–4998, 2013.

[11] R. Renju, C. S. Raju, N. Mathew, T. Antony, and K. K. Moorthy, "Microwave radiometer observations of interannual water vapor variability and vertical structure over a tropical station," *J. Geophys. Res. Atmos.*, vol. 120, no. 10, pp. 4585–4599, 2015.

[12] C. S. Raju, R. Renju, T. Antony, N. Mathew, and K. K. Moorthy, "Microwave radiometric observation of a waterspout over coastal Arabian Sea," *IEEE Geosci. Remote Sens. Lett.*, vol. 10, no. 5, pp. 1075–1079, Sep. 2013.

[13] Y. Han and E. R. Westwater, "Analysis and improvement of tipping calibration for ground-based microwave radiometers," *IEEE Trans. Geosci. Remote Sens.*, vol. 38, no. 3, pp. 1260–1276, May 2000.

[14] T. Hewison and C. Gaffard, "Radiometrics MP3000 microwave radiometer performance assessment," Met Office, Univ. Reading, Reading, U.K., Tech. Rep. TR 29, 2003.

[15] G. Xu, R. Ware, W. Zhang, G. Feng, K. Liao, and Y. Liu, "Effect of off-zenith observations on reducing the impact of precipitation on ground-based microwave radiometer measurement accuracy," *Atmos. Res.*, vols. 140–141, pp. 85–94, Apr./May 2014.

[16] P. Seibert, F. Beyrich, S.-E. Gryning, S. Joffre, A. Rasmussen, and P. Tercier, "Review and intercomparison of operational methods for the determination of the mixing height," *Atmos. Res.*, vol. 34, no. 7, pp. 1001–1027, 2000.

[17] K. Rajeev, K. Parameswaran, B. V. Thampi, M. K. Mishra, A. K. M. Nair, and S. Meenu, "Altitude distribution of aerosols over southeast Arabian Sea coast during pre-monsoon season: Elevated layers, long-range transport and atmospheric radiative heating," *Atmos. Environ.*, vol. 44, pp. 2597–2604, Jul. 2010.

[18] T. Luo, R. Yuan, and Z. Wang, "Lidar-based remote sensing of atmospheric boundary layer height over land and ocean," *Atmos. Meas. Techn.*, vol. 7, no. 1, pp. 173–182, 2014.

[19] J. R. Garratt, "The stably stratified internal boundary layer for steady and diurnally varying offshore flow," *Bound.-Layer Meteorol.*, vol. 38, no. 4, pp. 369–394, 1987.

R. Renju, photograph and biography not available at the time of publication.

C. Suresh Raju, photograph and biography not available at the time of publication.

M. K. Mishra, photograph and biography not available at the time of publication.

N. Mathew, photograph and biography not available at the time of publication.

K. Rajeev, photograph and biography not available at the time of publication.

K. Krishna Moorthy, photograph and biography not available at the time of publication.